journal of the mechanical behavior of biomedical materials 118 (2021) 104412

Contents lists available at ScienceDirect

Journal of the Mechanical Behavior of Biomedical Materials

journal homepage: www.elsevier.com/locate/jmbbm

Research paper

Modeling and application of anisotropic hyperelasticity of PDMS polymers with surface patterns obtained by additive manufacturing technology

Hoo Min Lee, Jaebum Sung, Byeongjo Ko, Heewon Lee, Sangyeun Park, Hongyun So, Gil Ho Yoon *

School of Mechanical Engineering, Hanyang University, Seoul, South Korea

ARTICLE INFO

Keywords:
Surface pattern
PDMS polymer
3D printer
Pattern angle
Pattern geometry
Property change
Soft robot

ABSTRACT

Polydimethylsiloxane (PDMS) polymer has been widely used in the biomedical fields because of its bio-compatibility, being used as sensors, medical equipment and tissue implants. The present study aims to synthesize and characterize micro lane-type surface patterns of PDMS polymers and evaluate their effects on mechanical properties for various applications in the bio-engineering field. Fabrication of surface patterns is achieved using fused filament fabrication in additive manufacturing, and the mechanical properties of the polymer specimens with the surface patterns are measured using tensile test. The surface patterns are rotated at different angles and changed into different shapes to change the anisotropic material properties of the PDMS specimens. This is achieved by changing the raster angles and modifying the fused filament paths during the additive manufacturing process. In addition, the application of the printed pattern to medical soft robot is presented. Owing to the anisotropic material properties, in-plane and out-of-plane actuation can be realized by attaching polymer patches with different lane-type surface patterns. The results of this study support the implementation of additive manufacturing for the rapid manufacture of scalable structures with anisotropic material properties for various applications.

1. Introduction

Elastomers have been thoroughly used in the biomedical fields due to their bio-mechanical characteristics such as bio-compatibility, flexibility and chemical stability. Among the elastomers, polydimethylsiloxane (PDMS) has stood up in the biomedical field for its ease in manufacturing process and low cost. Some of the application of PDMS polymers are sensors, electronic components, medical equipment and tissue implants (Victor et al., 2019). The present study aims to synthesize and characterize micro lane-type patterns of PDMS polymers, evaluate their effects on mechanical properties and apply to medical soft robot joint motion control. The surface patterns are fabricated by fused filament fabrication technique in 3D printing, and changes were made to the patterns by varying the raster angles and modifying the G-code during the additive manufacturing process. The mechanical properties of the manufactured specimens were measured using a tensile testing machine and analyzed to verify the effects of the micro-surface patterns. Mechanical modeling of the specimens with lane-type surface patterns was conducted using the anisotropic Mooney–Rivlin material model. To illustrate the application of the specimens, a simple application to soft robots is presented.

The changes in the mechanical properties of materials due to the variation of fiber directions have been a significant issue in different engineering fields (Coran et al., 1971; Tohgo et al., 1993; Cheng et al., 2020; Astruc et al., 2019; Morch et al., 2019). As additive manufacturing started to be utilized in recent years, some relevant researches covering wide range of materials such as metals, polymers, ceramics and composites (Surmeneva et al., 2020; Bourell et al., 2017) have been present in the additive manufacturing field. Various studies have been conducted on the effect of changing fused material orientation on the mechanical properties of the 3D printed products. Raster angles were varied to change the material orientations, and analyses of the tensile properties were performed on the specimens made of polylactic acid (PLA) (Kiendl and Gao, 2020; Lužanin et al., 2014; Ezeh and Susmel, 2019; Wu et al., 2017; Dizon et al., 2018; Zhao et al., 2019), and acrylonitrile butadiene styrene (ABS) (Ning et al., 2017; Wu et al., 2015; Huang and Singamneni, 2015). As additive manufacturing techniques have been utilized for various bio-engineering applications (Bose et al., 2018), the concept of raster angle variation was adopted in soft robot engineering (Connolly et al., 2015; Vignali et al., 2020; Kim et al., 2018; Su et al., 2019; Vanneste et al., 2020; Ahn et al., 2012) and

* Corresponding author.
E-mail address: ghy@hanyang.ac.kr (G.H. Yoon).

https://doi.org/10.1016/j.jmbbm.2021.104412
Received 26 November 2020; Received in revised form 17 February 2021; Accepted 17 February 2021
Available online 24 February 2021

flexible structure applications (Moroni et al., 2006; Shan et al., 2009). However, previous studies have reported the limitations in manufacturing efficiency, as the entire material orientation must be changed for property variation. Studies that consider the surface conditions were conducted to analyze the change in material properties (Manocha et al., 1988; Hong et al., 2005; Dai and Park, 2013; Hurtado and Ortiz, 2012), indicating that the variation of surface orientations can also induce property variations. As the inefficiency in manufacturing using raster angle variation becomes clear with increasing demand, it is necessary to improve the methods by applying the concept of surface modification. Over the last years, several studies were done on surface modification of PDMS polymers for manufacturing microfluidic devices (Zhou et al., 2012) and coating solid substrates (Eduok et al., 2017) to vary hydrophobic characteristics. Studies were also done on surface treating of PDMS polymers for encapsulation of sensors (Liu et al., 2016) to enhance photovoltaic performance. However, studies related to mechanical properties were not conducted even if tensile stresses are present in the following applications (Shemesh et al., 2015; Park et al., 2010). The anisotropic material properties observed in the present study may aid future studies related to tensile stresses in the applications. Therefore, this study aims to vary and control the mechanical properties using micro-surface patterns to improve manufacturing efficiency that lacked in the previous methods.

The fabrication of micro-surface patterns using 3D printing PLA molds has been introduced in past studies (Kang et al., 2019). The present study aims to use the micro-surface patterns to realize varying mechanical properties by changing pattern angle and geometry. A 3D printer prints PLA in the shape of a circular tube in micro units, forming lane-type patterns in a single direction on the surface of the printed structure. The direction of the lane-type patterns is varied by changing the raster angle, and the geometry of the patterns is varied by modifying the G-code for 3D printing. After printing the PLA molds with each characteristic surface pattern, polydimethylsiloxane (PDMS) polymer was poured into the PLA molds, baked to cure the pre-polymer, and detached to finalize the PDMS specimen with micro-scale surface patterns. The PDMS specimens were tested using a TXA tensile machine to measure the mechanical properties. The measured values of Young's modulus and hyper-elasticity were analyzed to determine the effects of surface patterns on the mechanical properties of the PDMS specimen. In addition, the application of the printed pattern to soft robot is presented. Owing to the anisotropic material properties, in-plane and out-of-plane actuation can be realized by attaching patches onto the surfaces of the actuators. The experiments in this study may aid the use of additive manufacturing for the rapid manufacture of scalable structures with anisotropic material properties for various applications.

The remainder of this paper is organized as follows. Section 2 provides some background to the casting approach for the lane-type pattern and the experimental method for material properties. In Section 3, the mechanical properties of the rotated lane-type pattern are measured and presented; the modification of the G-code for an additive manufacturing approach is also presented. Section 4 presents the simple application of the soft robot using the PDMS micro-pattern specimen. Conclusions and future research topics are discussed in Section 5.

2. Experimental section

2.1. Materials

To prepare a casting mold with lane-type micro-surface patterns, flat molds were designed using computer-aided design software and printed using the Creality Ender 3 Pro printer shown in Fig. 1. The printing conditions of printing speed, extruder temperature, and platform temperature were set as 50 mm/s, 200 °C, and 50 °C, respectively. The infill density was set as 20% to minimize the printing time, while ensuring that the details required for the molds were maintained. The eSUN PLA 3D printer filament of 1.75 mm diameter was used to print the PLA molds. The layer height of the printed PLA was determined to be 0.300 mm.

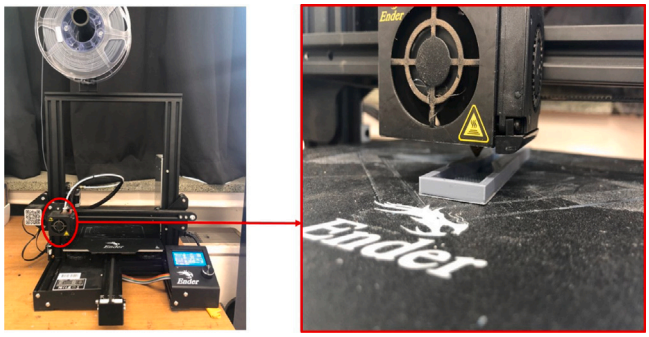

Fig. 1. 3D printer for manufacturing of PLA mold.

Fig. 2 illustrates the fabrication process for PDMS polymer specimens using the printed PLA molds. Casting molds were printed with different raster angles between 0° and 90°. The mold bodies were designed to have length of 120 mm, width of 25 mm and height of 6 mm. The printing of PLA filament in the shape of circular tubes induced the surfaces of the printed products to naturally gain straight lane-type surface patterns. PDMS pastes, made using Dow Corning Sylgard 184 base elastomer and curing agent, were poured into the printed molds with the surface patterns. The PDMS pastes were baked at 45 °C for 7 h to cure the pre-polymer and separate them from the molds. The PDMS specimens detached themselves from the PLA molds easily without any further treatment between the mold surfaces and specimens. As the manufacturing process did not damage the 3D printed molds, the molds could be repeatedly used to manufacture identical PDMS polymer specimens, supporting the rapid, cost-effective, and efficient manufacturing method to realize the micro-surface patterns. Finally, the mechanical properties of the detached PDMS specimens were characterized experimentally.

Fig. 3 illustrates the manufactured PDMS specimens with surface patterns in different orientations and shows the actual surface patterns of each PDMS specimen. Five pattern types were printed using mold casting method, each having pattern angles of 90°, 60°, 45°, 30°, and 0°. The PDMS specimens were made to conduct tensile tests to investigate the mechanical properties. The gauge length, gauge width, and the thickness values of the specimens were designed to be 25 mm, 6 mm and 5 mm respectively. The thickness values of surface patterns were designed to be 0.300 mm, making the ratio of the surface pattern thickness to the total specimen thickness to be 1:16.

2.2. Testing and characterization

The tensile tests were conducted using the TXA^{TM} Standard Texture Analyzer supplied by YEONJIN S-Tech Corporation. Using the TXA tensile tester depicted in Fig. 4, the mechanical properties of the manufactured PDMS specimens were tested and measured at a loading rate of 1 mm/min. To obtain accurate properties, ten specimens for each surface pattern were tested, and the mean values were evaluated.

The testing process consisted of two parts. The first part was the tensile test of the PDMS specimens in the elastic region, in which temporary deformations were produced. In this section, the stiffness of the specimens was investigated by determining the relationship between the raster angles and Young's modulus. The second part was the tensile test of the PDMS specimens over the elastic region, in which minor permanent deformations were observed. The test was conducted until the change in length of the specimen reached 25 mm. In this section, the hyper-elasticity of the specimens was investigated by finding suitable material parameters of the anisotropic Mooney–Rivlin model. Overall, a tensile test using a TXA texture analyzer was conducted to investigate the effect of surface patterns on the changes in the mechanical properties of the PDMS specimens.

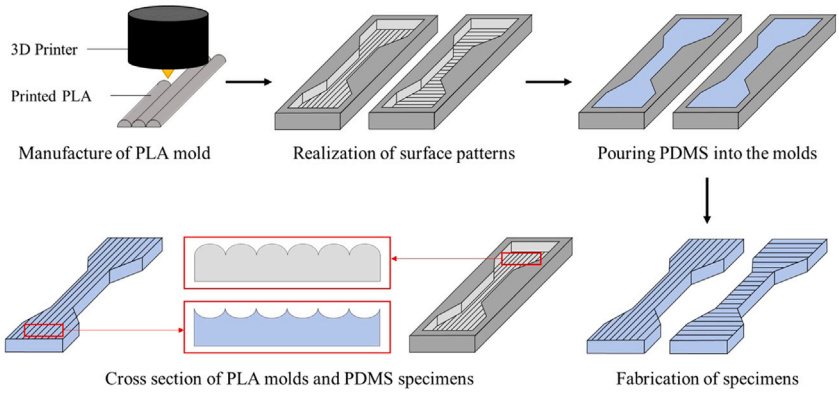

Fig. 2. Illustration of the fabrication process for PDMS polymers with micro-scale surface patterns.

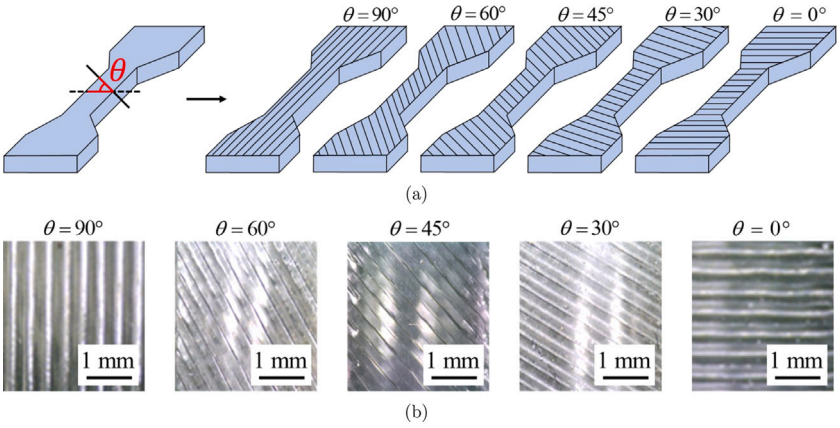

Fig. 3. Illustration of PDMS specimen made of different raster angles for tensile test: (a) orientation of lane-type patterns and (b) enlarged pictures of surface patterns.

Fig. 4. TXA texture analyzer for tensile test of PDMS specimen.

3. Results and discussions

3.1. Influence of raster angle on Young's modulus

Tensile tests demonstrated the effect of aligned cylinder surface patterns on Young's modulus. Results of tensile test are presented in the form of stress–strain curve in Fig. 5a. The results show the mean values of 10 experiments for each pattern. The curves depict the elastic deformation region with the slopes representing the Young's modulus values for each type of specimen. From the results, the highest Young's modulus for the specimens are observed with the 90° orientation surface pattern, followed by the specimens with 60°, 45°, and 30° surface pattern orientations. The specimens with the 0° surface pattern orientation had the lowest Young's modulus. The relationship between the raster angles and Young's modulus of the PDMS specimens is presented in Fig. 5b. The two variables are positively correlated. The mean Young's modulus value increases when the raster angle increases from 0° to 90°. The average Young's modulus value of the PDMS specimen with a 0° pattern angle is approximately 4.58 MPa, while the average Young's modulus value of the PDMS specimen with a 90° pattern angle is approximately 5.73 MPa. This indicates that the Young's modulus value can be increased by approximately 25% by changing the orientation of its surface pattern. In short, the experiments show an increase in Young's modulus because of the aligned cylinder structures.

3.2. Influence of raster angle on anisotropic hyperelasticity of specimen

In addition to the Young's modulus, anisotropic hyperelasticity is considered. The PDMS specimens can be extended over the elastic region, where geometrical nonlinearity and material nonlinearity are observed. The representative curves are demonstrated in Fig. 6. As the focal points exist beyond the elastic regions, the Mooney–Rivlin model can be adopted.

Owing to the anisotropic properties of the specimens and the large displacements, the following anisotropic Mooney–Rivlin model is implemented. The parameters of this mathematical model can be determined by adjusting the stress–strain curves obtained experimentally. The strain energy function for the anisotropic Mooney–Rivlin model is expressed as follows (Tang et al., 2007):

$$W = C_1(I_1 - 3) + C_2(I_2 - 3) + D_1(e^{[D_2(I_1-3)]} - 1) + \frac{K_1}{2K_2} e^{[K_2(I_4-1)^2-1]} \quad (1)$$

$$I_1 = \mathrm{tr}(\mathbf{C}),\ I_2 = \frac{1}{2}\left[\{\mathrm{tr}(\mathbf{C})\}^2 - \mathrm{tr}(\mathbf{C}^2)\right],\ I_4 = \mathbf{a}^{\mathrm{T}} \cdot \mathbf{C} \cdot \mathbf{a} \quad (2)$$

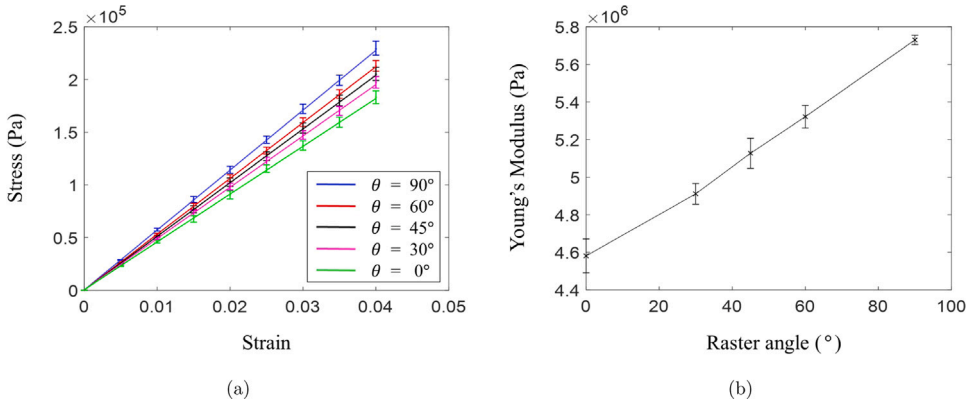

Fig. 5. Tensile experiments: (a) Stress–strain curve of PDMS specimens and (b) the relationship between the raster angle and Young's modulus.

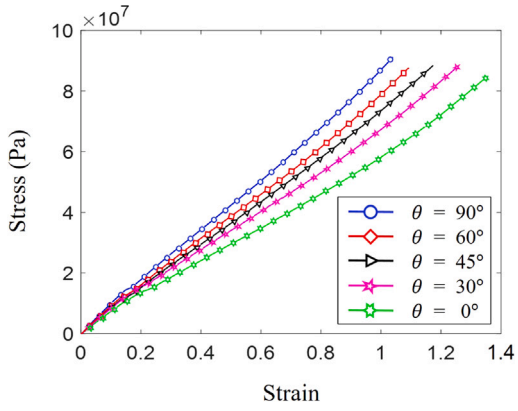

Fig. 6. Results of tensile experiments: Stress–strain curve of PDMS specimen with different surface patterns to exhibit hyperelasticity.

where I_1, I_2 and I_4 are the first, second, and fourth strain invariants, respectively. The normalized vector of the surface pattern direction and the right Cauchy–Green deformation tensor are denoted by **a** and **C**, respectively. The right Cauchy–Green deformation tensor can be defined as follows:

$$\mathbf{C} = \begin{bmatrix} \lambda_1^2 & 0 & 0 \\ 0 & \lambda_2^2 & 0 \\ 0 & 0 & \lambda_3^2 \end{bmatrix} (\lambda_i = 1 + \varepsilon_i, i = 1, 2 \text{ and } 3) \tag{3}$$

where λ_i and ε represent the stretch value in the principal direction and strain, respectively. As the tensile tests are conducted uniaxially, the stretch components for the three principal directions can be defined as follows:

$$\lambda_1 = \lambda,\ \lambda_2 = \frac{1}{\sqrt{\lambda}},\ \lambda_3 = \frac{1}{\sqrt{\lambda}} \tag{4}$$

where the stretch component in the direction of the tensile test is denoted by λ. The stress can be expressed as follows:

$$\sigma = \frac{\mathrm{d}W}{\mathrm{d}\varepsilon} \tag{5}$$

The material parameters C_1, C_2, D_1, D_2, K_1, and K_1 in Eq. (2) can be identified by fitting the anisotropic Mooney–Rivlin model to the experimental stress–strain curves presented in Fig. 6. Without the loss of generality, the present study determines the coefficient values of the anisotropic Mooney–Rivlin model, listed in Table 1 with respect to the rotation angle θ using the least square scheme. Similar values can be obtained with certain deviations due to the manufacturing tolerance, deviation in measurement, etc. For the representative values of these coefficients of the anisotropic Mooney–Rivlin model, the average values are computed and used throughout this research. Fig. 7 illustrates the curve fit of the anisotropic Mooney–Rivlin model with the values presented in Table 1, and the estimated coefficients are suitable to interpolate the stress–strain curves with respect to the pattern angle.

However, some differences exist, but similar values can be obtained in Table 1. From our analysis, the errors obtained are confined to within 7% of the mean values, which shows the reliability of the specimens. In addition, this indicates that the anisotropic Mooney–Rivlin model is suitable for modeling the mechanical behavior of the specimens in the presence of surface patterns.

3.3. Extension to wave-type pattern

As an extension of the present study, the wave-type pattern shown in Fig. 8 was fabricated. The existing 3D printer only allows the lane-type patterns with rotational angles. Therefore, to develop the wave pattern, the surface contacting the PDMS solution was changed by modifying the G-code directly. Furthermore, printing conditions, such as extrusion temperature and printing speed, were optimized to obtain a clear surface pattern. Fig. 8 illustrates the manufacturing process of the PLA mold with the wave pattern.

Except for the manual generation of the G-code, the fabrication process of the PDMS specimen with wave pattern afterwards was identical to that of the specimens with lane-type patterns. A PDMS mixture of pre-polymer and curing agent was poured into the printed molds and baked at 45 °C for 7 h. The detached PDMS specimens were characterized to demonstrate changes in the mechanical properties. Fig. 8 illustrates the manufactured PDMS specimens with wave patterns. The wave patterns were fabricated to have a pattern angle of 90°, to observe how the change in geometry of the surface patterns influences the mechanical properties in comparison to the lane-type patterns with identical pattern angles. The same tensile tests were performed for the wave pattern specimens using the TXA texture analyzer. The stress–strain curve is presented in Fig. 9.

In Fig. 9a, it can be observed that the Young's modulus of the PDMS specimen with the wave pattern is approximately 5.06 MPa, which is closest to the Young's modulus value of the PDMS specimen having the lane-type pattern with 45° (5.13 MPa). In Fig. 9b, it can be observed that the stress–strain curve for the hyperelastic model has a single focal point, showing similar tendency with those of the lane-type pattern specimens. The material parameters of the anisotropic Mooney–Rivlin model presented in Table 1 are used to find the normalized vector of the surface pattern direction **a** of the wave pattern. Using **a**, it is possible to identify which pattern angle of the lane-type pattern has a similar effect as the wave pattern.

The four terms in Eq. (1) are formulated to consider the physical stress–strain curves. The last term related to the fourth strain invariant I_4 is the anisotropic term that changes the strain energy with respect to the direction of the surface pattern, as the fourth strain invariant is

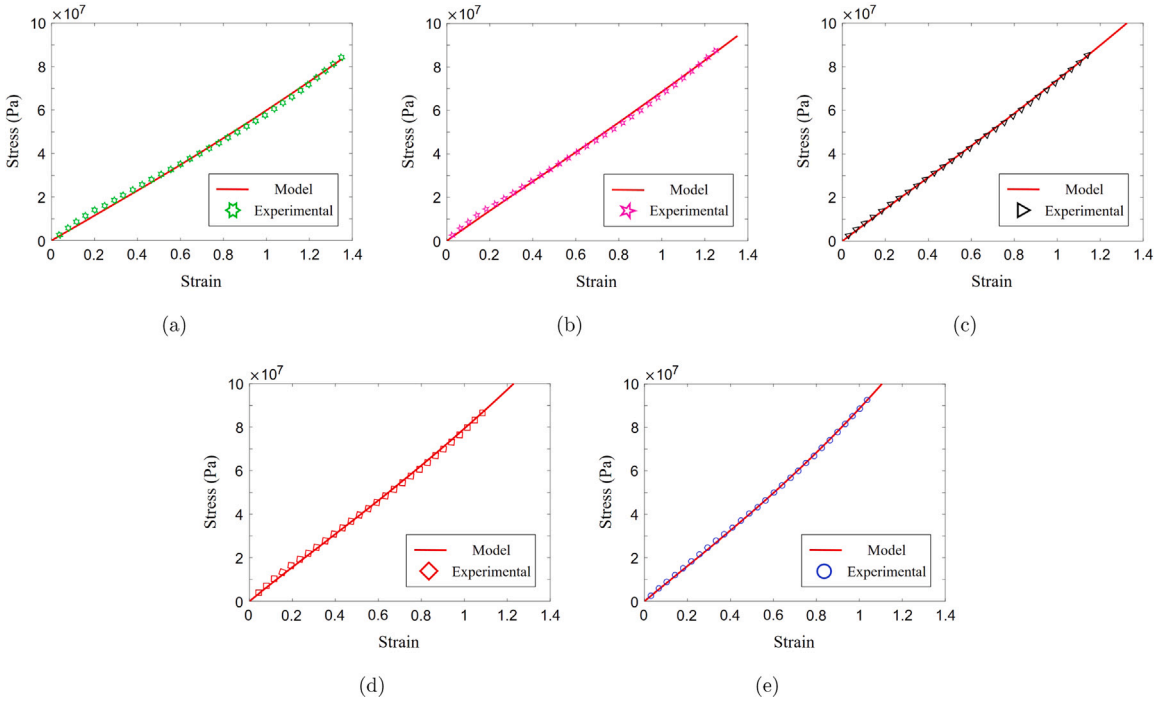

Fig. 7. Comparisons of the stress–strain curves of the experimental results and anisotropic Mooney–Rivlin model with the coefficients in Table 1: Pattern angle of (a) 0°, (b) 30°, (c) 45°, (d) 60°, and (e) 90°.

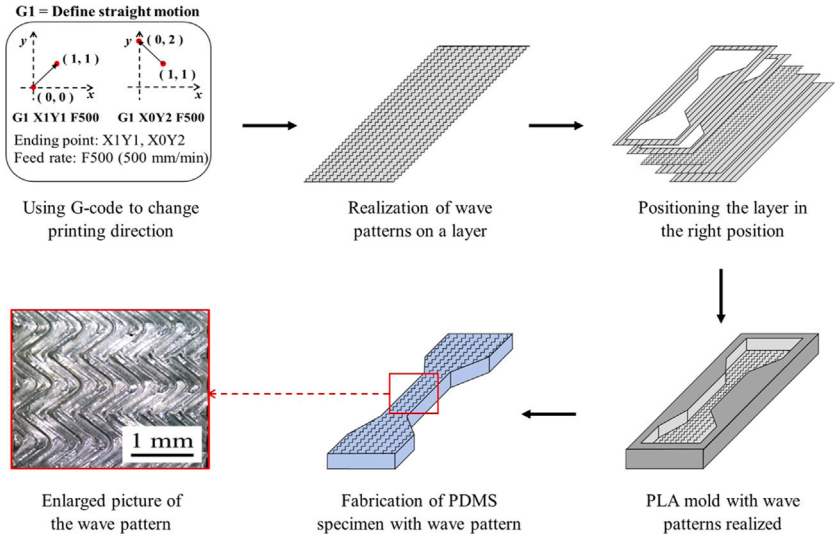

Fig. 8. The manufacturing process of the wave pattern mold and the end product with wave pattern.

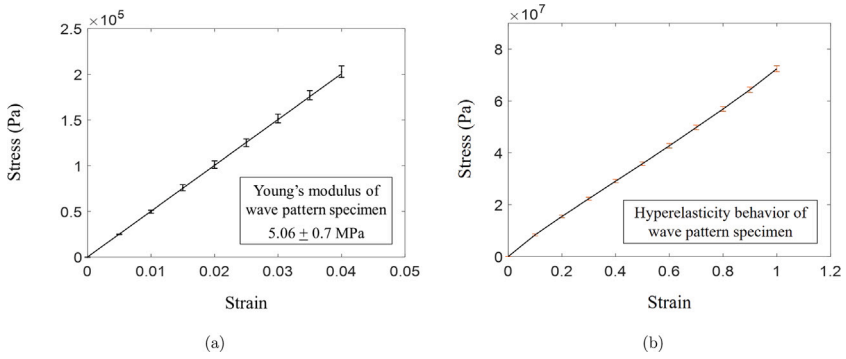

Fig. 9. Results of wave pattern specimen: (a) Stress–strain curve of PDMS specimen in elastic region and (b) stress–strain curve of PDMS specimen over elastic region.

Table 1
Coefficient values of the anisotropic Mooney–Rivlin model for the different surface patterns.

Surface pattern	$C_1/10^7$ (Pa)	$C_2/10^6$ (Pa)	$D_1/10^7$ (Pa)	$D_2/10^{-1}$	$K_1/10^6$ (Pa)	$K_2/10^{-3}$
$\theta = 0°$	2.3332	−9.0926	1.1048	−3.1680	5.3525	2.1000
$\theta = 30°$	2.5123	−9.0926	1.1048	−3.1678	5.3525	2.1000
$\theta = 45°$	2.6127	−9.0926	1.1048	−3.1678	5.3525	2.1000
$\theta = 60°$	2.5514	−9.0926	1.1048	−3.1680	5.3525	2.1000
$\theta = 90°$	2.4903	−9.0926	1.1048	−3.1678	5.3525	2.1000
Mean value	2.5000	−9.0926	1.1048	−3.1679	5.3525	2.1000

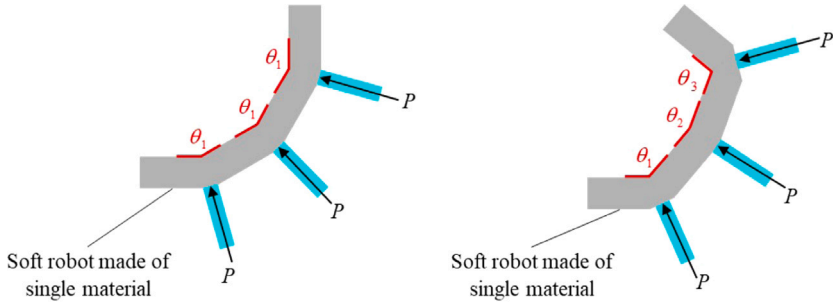

(a) Present mechanism of soft robots (b) Desired mechanism of soft robots

Fig. 10. Mechanism of soft robot using air actuators: (a) The uniform bending deformation and (b) the different bending deformation.

a function of the normalized fiber direction vector **a**. Specifically, the pattern angle θ_w can be defined as follows:

$$\mathbf{a}_w = \begin{pmatrix} x \\ y \\ 0 \end{pmatrix}, \quad \theta_w = \tan^{-1}\left(\frac{x}{y}\right) \tag{6}$$

where θ_w for the lane-type pattern has similar effects to that of the wave pattern (90°). Accordingly, the following relations can be defined:

$$I_{4,w} = \mathbf{a}_w^{\mathrm{T}} \cdot \mathbf{C} \cdot \mathbf{a}_w = x^2\lambda^2 + \frac{y^2}{\lambda} \tag{7}$$

By substituting Eq. (7) and the mean values of the material parameters listed in Table 1 into Eq. (1) , the component values of x and y are evaluated to be 6.6524×10^{-1} and 7.4663×10^{-1}, respectively. The calculated value of θ_w is approximately 41.7°, indicating that the wave pattern has the same effect as the lane-type pattern with a 41.7° pattern angle in terms of the hyperelasticity. Interestingly, a similar observation can be made for the Young's modulus. Moreover, the Young's modulus of the specimen with the wave pattern lies between that of the 30° and 45° lane-type patterns.

The tendency of the wave pattern with a 90° pattern angle exhibits similar results with the lane-type pattern having a 45° pattern angle; this may be due to the fact that the wave pattern consists of continuous 45° lane-type patterns. Overall, the changes in pattern geometry prove to serve as another parameter in changing the mechanical properties of PDMS specimens, where both the tensile strength and hyperelasticity change due to the changes in pattern geometry.

4. Engineering application

This section applies the micro-patterns to medical soft robots, enabling enhanced robot movement and delicate motion control, as illustrated in Fig. 10. One of the common actuators of soft robots in medical applications is the pneumatic actuator by vacuum or compressed air, and constant pressure is developed inevitably inside the soft materials (Tse et al., 2018). For example, Fig. 10a shows an example with constant pressure and a soft robot of uniform thickness, in which uniform deformations occur. However, existing soft robots have limitations in having to change the input pressure of the pneumatic actuator when the bending angles of the joints change. This indicates that each joint of the soft robot must have individual air actuators to control the motion of the robot, thereby compromising its inefficiency.

For enhanced motion, different pressure should be applied. To enhance the motion of a soft robot subjected to constant pressure, the material properties of the soft robot can be varied, as shown in Fig. 10b by attaching the specimens with the surface patterns. This indicates that joint parts do not require individual air actuators, thus increasing the efficiency in controlling soft robot motions. Moreover, more delicate motion control can be achieved by engraving the surface patterns of appropriate pattern angles and pattern geometries at the joints of soft robots.

To validate the concept of the application of the lane-type PDMS specimens to soft robots, experiments were conducted as illustrated in Fig. 11. To attach the specimens, they were cut into 10 mm × 5mm rectangular patches with 2 mm thickness. The pattern angles were varied to 0°, 30°, 45°, 60°, and 90°. The soft robots with the patches were expanded at constant air pressure, as shown in Fig. 11.

The experiments in Fig. 12 show that the pattern angles of lane type patterns affect the bending motion of balloons with the PDMS specimens. Because of the specimens with pattern angles of 30°, 45°, and 60°, the balloons showed bending motions in the x-direction and rotational motion in the y-direction with rotation angles of 8.7°, 6.3°, and 10.3°, respectively. However, PDMS specimens with pattern angles of 0° and 90° forced the balloons to undergo bending motion in the x-axis with small rotation around the y-axis with rotation angles of 0.7° and 0.5°, respectively. The difference in the pattern angles of the identical lane-type patterns led to different rotation angles of the balloons, indicating that surface patterns can be utilized to vary the rotating motion in soft robot applications.

While the experiment showed that the differences in surface patterns lead to differences in the rotating angles, no differences in bending angles were found in the process. All balloons had similar bending angles between 33° and 35°. This indicates that several other factors affect the bending angle of the balloons, while pattern angles affect the rotation angle. To investigate the factors that affect the bending angles, further experiments were performed. In this experiment, the PDMS specimens were fabricated to have different values of length and width. The experiment was performed using the same method.

Fig. 13 presents the results of the experiment. PDMS specimens of 60° pattern angle were used for all cases. The red, yellow, and blue balloons were attached with specimens of different sizes, each having lengths of 10 mm, 5 mm, and 10 mm, respectively and widths of 5 mm, 5 mm, and 2.5 mm, respectively. Consequently, the red balloon had the

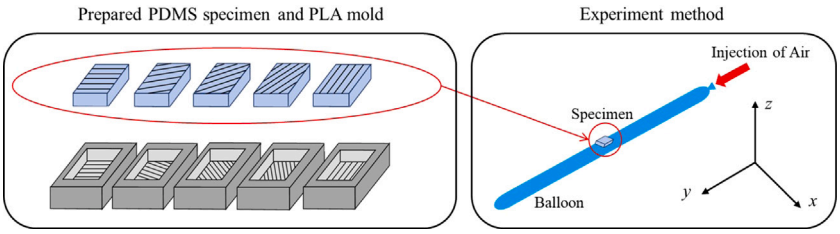

Fig. 11. Application of PDMS specimen and balloon on soft robot experiment.

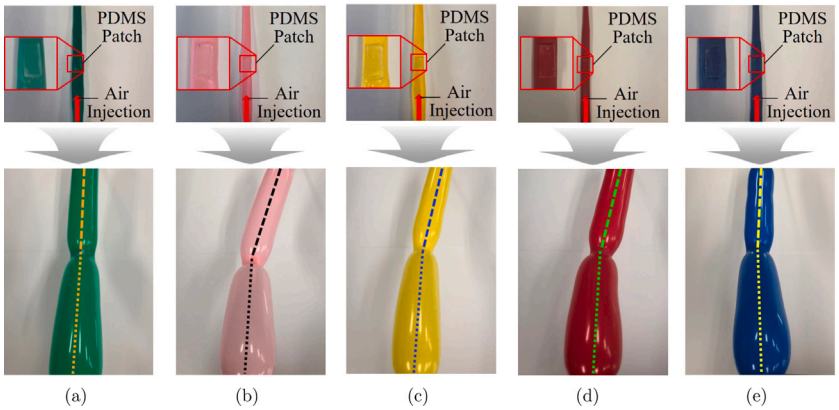

Fig. 12. Experiment results regarding rotating angles: Surface patterns of (a) 0°, (b) 30°, (c) 45°, (d) 60°, and (e) 90°.

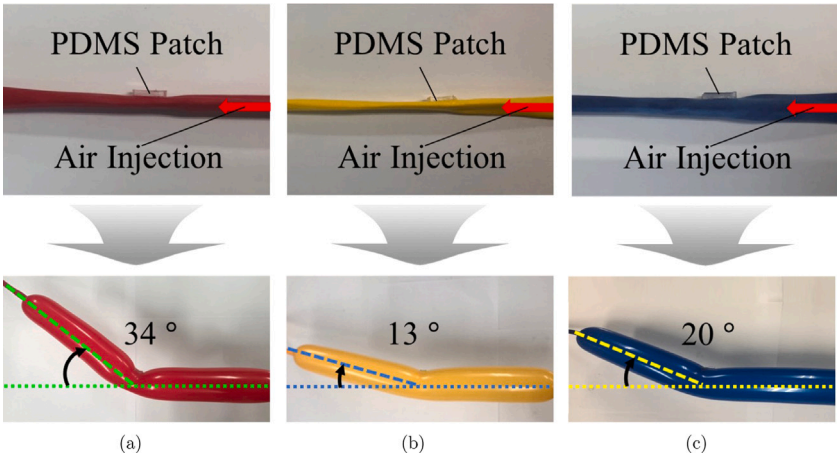

Fig. 13. Experiment results regarding bending angles: Specimens of (a) 10 mm length and 5 mm width, (b) 5 mm length and 5 mm width, and (c) 10 mm length and 2.5 mm width.

greatest bending angle of 34°; meanwhile, the yellow and blue balloons had bending angles of 13° and 20°, respectively. When the length and width of the specimen were halved, the bending angle decreased by 62% and 52%, respectively. This experiment reveals that rather than the pattern angle of the PDMS specimen, the length and width of the PDMS specimen affect the bending angle, indicating that the surface patterned area affects the degree of bending.

The experiments successfully show that the micro-surface patterns created by 3D printing can be applied to soft robots; to provide variations to joint motions. Even when air was injected at constant pressure, both the degree of rotation around the y-axis and the bending in the x-axis were varied by changing the surface pattern angles and surface patterned area. This indicates that soft robot motions can be controlled by applying appropriate surface patterns to each joint of the robot. The soft robot mechanism using air actuators can be improved, as individual air actuators for each joint part can be replaced with a single air actuator, thereby increasing the efficiency of controlling soft robot motions.

5. Conclusions

This study focuses on the changes in mechanical properties of PDMS polymers that arise from micro surface patterns created by additive manufacturing. The variation in the mechanical properties of materials is a significant issue in several engineering applications. To address this from an additive manufacturing perspective, this study develops a new manufacturing method with micro surface patterns using fused filament 3D printing and investigates the change in the material properties by the anisotropic hyperelasticity model. The fabrication of the surface patterns is realized by additive manufacturing, where PLA is printed in circular tubes to create lane-type patterns in a single direction. The pattern angle and pattern geometry can be modified by varying the raster angle and G-code. PDMS specimens with surface patterns were

Strain	Stress applied to straight pattern (0°)	Stress applied to straight pattern (30°)	Stress applied to straight pattern (45°)	Stress applied to straight pattern (60°)	Stress applied to straight pattern (90°)	Stress applied to wave pattern
0.005	22.8 ± 0.3 KPa	23.6 ± 0.2 KPa	25.6 ± 0.4 KPa	26.5 ± 0.3 KPa	28.5 ± 0.3 KPa	24.9 ± 0.4 KPa
0.010	45.8 ± 1.0 KPa	49.1 ± 1.1 KPa	49.8 ± 1.7 KPa	53.2 ± 1.0 KPa	57.3 ± 1.6 KPa	49.6 ± 1.7 KPa
0.015	67.8 ± 3.2 KPa	73.5 ± 2.7 KPa	76.8 ± 3.4 KPa	79.9 ± 2.7 KPa	86.1 ± 3.4 KPa	75.8 ± 3.4 KPa
0.020	90.5 ± 3.8 KPa	98.2 ± 3.2 KPa	102.5 ± 4.1 KPa	106.4 ± 3.1 KPa	114.6 ± 4.0 KPa	101.1 ± 4.1 KPa
0.025	115.4 ± 3.9 KPa	122.7 ± 3.6 KPa	127.2 ± 4.2 KPa	132.6 ± 3.3 KPa	143.1 ± 4.2 KPa	125.0 ± 4.2 KPa
0.030	137.4 ± 4.5 KPa	147.3 ± 4.1 KPa	153.9 ± 4.8 KPa	159.6 ± 4.0 KPa	172.0 ± 4.8 KPa	151.6 ± 4.8 KPa
0.035	159.4 ± 4.8 KPa	170.1 ± 4.2 KPa	180.1 ± 5.1 KPa	186.3 ± 4.1 KPa	198.9 ± 5.1 KPa	177.1 ± 5.1 KPa
0.040	183.1 ± 6.1 KPa	197.0 ± 5.5 KPa	205.1 ± 6.3 KPa	212.9 ± 5.1 KPa	229.2 ± 6.2 KPa	202.7 ± 6.3 KPa

Fig. A.14. Stress values in the elastic region for all specimens.

Strain	Stress applied to straight pattern (0°)	Stress applied to straight pattern (30°)	Stress applied to straight pattern (45°)	Stress applied to straight pattern (60°)	Stress applied to straight pattern (90°)	Stress applied to wave pattern
0.10	5.4 ± 0.1 MPa	5.8 ± 0.1 MPa	6.0 ± 0.1 MPa	6.5 ± 0.1 MPa	7.3 ± 0.1 MPa	5.9 ± 0.1 MPa
0.20	13.7 ± 0.2 MPa	14.6 ± 0.3 MPa	15.2 ± 0.3 MPa	16.1 ± 0.3 MPa	17.8 ± 0.3 MPa	15.0 ± 0.3 MPa
0.30	18.6 ± 0.3 MPa	21.4 ± 0.4 MPa	22.6 ± 0.4 MPa	23.9 ± 0.4 MPa	26.3 ± 0.4 MPa	22.2 ± 0.4 MPa
0.40	24.1 ± 0.4 MPa	27.7 ± 0.5 MPa	29.5 ± 0.6 MPa	31.5 ± 0.5 MPa	34.3 ± 0.5 MPa	28.9 ± 0.6 MPa
0.50	29.5 ± 0.6 MPa	34.0 ± 0.6 MPa	36.4 ± 0.7 MPa	38.7 ± 0.6 MPa	42.3 ± 0.6 MPa	35.0 ± 0.7 MPa
0.60	34.7 ± 0.7 MPa	40.3 ± 0.8 MPa	43.4 ± 0.8 MPa	45.9 ± 0.8 MPa	50.4 ± 0.7 MPa	42.4 ± 0.8 MPa
0.70	40.4 ± 0.7 MPa	46.6 ± 0.9 MPa	50.7 ± 0.9 MPa	53.5 ± 0.9 MPa	58.9 ± 0.8 MPa	48.3 ± 1.0 MPa
0.80	46.0 ± 0.9 MPa	53.1 ± 1.0 MPa	58.0 ± 1.0 MPa	61.4 ± 0.9 MPa	67.9 ± 0.9 MPa	56.5 ± 1.0 MPa
0.90	51.9 ± 1.0 MPa	60.0 ± 1.1 MPa	65.5 ± 1.2 MPa	69.9 ± 1.1 MPa	77.0 ± 1.0 MPa	63.9 ± 1.2 MPa
1.00	58.1 ± 1.1 MPa	67.3 ± 1.3 MPa	73.5 ± 1.4 MPa	78.9 ± 1.3 MPa	87.0 ± 1.2 MPa	71.7 ± 1.3 MPa

Fig. B.15. Stress values over the elastic region for all specimens.

fabricated by pouring PDMS polymer into the PLA molds, baking to cure the pre-polymer and detaching from the molds. Tensile tests of the PDMS specimens were conducted using a TXA tensile machine. The anisotropic hyperelasticity model was adopted, and the involved parameters were determined, examined, and analyzed. From an engineering application, this research presents the enhancement of soft robot motion with PDMS specimens. To prove this concept, experiments were conducted to validate the motion control of soft robot joints using PDMS specimens with different surface patterns, and it has been proven possible to change the bending angles and rotating angles of soft robot joints. For future research, the optimization of pattern angles and pattern geometry, considering delicate motion control of soft robots, can be studied, for more practical issues. Furthermore, the experimental analysis can be improved by considering other mechanical properties, such as compressive properties. In short, the research successfully presents a new method in additive manufacturing to fabricate surface patterns, investigates the anisotropic hyperelasticity properties, and applies it to soft robot examples.

CRediT authorship contribution statement

Hoo Min Lee: Prepare the specimens and conduct the experiments, Mainly carries out the experiment, Prepare a draft. **Jaebum Sung:** Prepare the specimens and conduct the experiments. **Byeongjo Ko:** Prepare the specimens and conduct the experiments. **Heewon Lee:** Prepare the specimens and conduct the experiments. **Sangyeun Park:** Prepare the specimens and conduct the experiments. **Hongyun So:** Discuss the material, Discuss the direction of the study. **Gil Ho Yoon:** Discuss the material, Discuss the direction of the study.

Declaration of competing interest

The authors declare that they have no known competing financial interests or personal relationships that could have appeared to influence the work reported in this paper.

Acknowledgment

This work was supported by the National Research Foundation of Korea (NRF) grant funded by the Korean government (MSIT) (NRF-2019R1A2C2084974).

Appendix A. Stress values in the elastic region

Table for the mean stress values with standard deviations in the elastic region in Fig. A.14.

Appendix B. Stress values over the elastic region

Table for mean stress values with standard deviations over the elastic region in Fig. B.15.

References

Ahn, S.-H., Lee, K.-T., Kim, H.-J., Wu, R., Kim, J.-S., Song, S.-H., 2012. Smart soft composite: An integrated 3D soft morphing structure using bend-twist coupling of anisotropic materials. Int. J. Precis. Eng. Manuf. 13 (4), 631–634.

Astruc, L., Morch, A., Witz, J.-F., Nováček, V., Turquier, F., Hoc, T., Brieu, M., 2019. An anisotropic micro-ellipsoid constitutive model based on a microstructural description of fibrous soft tissues. J. Mech. Phys. Solids 131, 56–73.

Bose, S., Ke, D., Sahasrabudhe, H., Bandyopadhyay, A., 2018. Additive manufacturing of biomaterials. Prog. Mater. Sci. 93, 45–111.

Bourell, D., Kruth, J.P., Leu, M., Levy, G., Rosen, D., Beese, A.M., Clare, A., 2017. Materials for additive manufacturing. CIRP Ann. 66 (2), 659–681.

Cheng, J., Jia, Z., Li, T., 2020. A constitutive model of microfiber reinforced anisotropic hydrogels: With applications to wood-based hydrogels. J. Mech. Phys. Solids 138, 103893.

Connolly, F., Polygerinos, P., Walsh, C.J., Bertoldi, K., 2015. Mechanical programming of soft actuators by varying fiber angle. Soft Robot. 2 (1), 26–32.

Coran, A., Boustany, K., Hamed, P., 1971. Unidirectional fiber–polymer composites: Swelling and modulus anisotropy. J. Appl. Polym. Sci. 15 (10), 2471–2485.

Dai, S., Park, H.S., 2013. Surface effects on the piezoelectricity of zno nanowires. J. Mech. Phys. Solids 61 (2), 385–397.

Dizon, J.R.C., Espera Jr, A.H., Chen, Q., Advincula, R.C., 2018. Mechanical characterization of 3D-printed polymers. Addit. Manuf. 20, 44–67.

Eduok, U., Faye, O., Szpunar, J., 2017. Recent developments and applications of protective silicone coatings: A review of pdms functional materials. Prog. Org. Coat. 111, 124–163.

Ezeh, O., Susmel, L., 2019. Fatigue strength of additively manufactured polylactide (PLA): effect of raster angle and non-zero mean stresses. Int. J. Fatigue 126, 319–326.

Hong, Z., Zhang, P., He, C., Qiu, X., Liu, A., Chen, L., Chen, X., Jing, X., 2005. Nano-composite of poly (l-lactide) and surface grafted hydroxyapatite: mechanical properties and biocompatibility. Biomaterials 26 (32), 6296–6304.

Huang, B., Singamneni, S., 2015. Raster angle mechanics in fused deposition modelling. J. Compos. Mater. 49 (3), 363–383.

Hurtado, D.E., Ortiz, M., 2012. Surface effects and the size-dependent hardening and strengthening of nickel micropillars. J. Mech. Phys. Solids 60 (8), 1432–1446.

Kang, B., Sung, J., So, H., 2019. Realization of superhydrophobic surfaces based on three-dimensional printing technology. Int. J. Precis. Eng. Manuf. Green Technol. 1–9.

Kiendl, J., Gao, C., 2020. Controlling toughness and strength of FDM 3D-printed PLA components through the raster layup. Composites B 180, 107562.

Kim, H., Lee, H., Ha, I., Jung, J., Won, P., Cho, H., Yeo, J., Hong, S., Han, S., Kwon, J., et al., 2018. Biomimetic color changing anisotropic soft actuators with integrated metal nanowire percolation network transparent heaters for soft robotics. Adv. Funct. Mater. 28 (32), 1801847.

Liu, Z., Sun, B., Shi, T., Tang, Z., Liao, G., 2016. Enhanced photovoltaic performance and stability of carbon counter electrode based perovskite solar cells encapsulated by pdms. J. Mater. Chem. A 4 (27), 10700–10709.

Lužanin, O., Movrin, D., Plančak, M., 2014. Effect of layer thickness, deposition angle, and infill on maximum flexural force in fdm-built specimens. J. Technol. Plast. 39 (1), 49–58.

Manocha, L.M., Yasuda, E., Tanabe, Y., Kimura, S., 1988. Effect of carbon fiber surface-treatment on mechanical properties of c/c composites. Carbon 26 (3), 333–337.

Morch, A., Astruc, L., Witz, J.-F., Lesaffre, F., Lecomte-Grosbras, P., Soulat, D., Brieu, M., 2019. Modeling of anisotropic hyperelastic heterogeneous knitted fabric reinforced composites. J. Mech. Phys. Solids 127, 47–61.

Moroni, L., De Wijn, J., Van Blitterswijk, C., 2006. 3d fiber-deposited scaffolds for tissue engineering: influence of pores geometry and architecture on dynamic mechanical properties. Biomaterials 27 (7), 974–985.

Ning, F., Cong, W., Hu, Y., Wang, H., 2017. Additive manufacturing of carbon fiber-reinforced plastic composites using fused deposition modeling: Effects of process parameters on tensile properties. J. Compos. Mater. 51 (4), 451–462.

Park, C.-s., Han, Y., Joo, K.-I., Lee, Y.W., Kang, S.-W., Kim, H.-R., 2010. Optical detection of volatile organic compounds using selective tensile effects of a polymer-coated fiber bragg grating. Opt. Express 18 (24), 24753–24761.

Shan, Y., Philen, M., Lotfi, A., Li, S., Bakis, C.E., Rahn, C.D., Wang, K.-W., 2009. Variable stiffness structures utilizing fluidic flexible matrix composites. J. Intell. Mater. Syst. Struct. 20 (4), 443–456.

Shemesh, J., Jalilian, I., Shi, A., Yeoh, G.H., Tate, M.L.K., Warkiani, M.E., 2015. Flow-induced stress on adherent cells in microfluidic devices. Lab Chip 15 (21), 4114–4127.

Su, M., Xie, R., Zhang, Y., Kang, X., Huang, D., Guan, Y., Zhu, H., 2019. Pneumatic soft actuator with anisotropic soft and rigid restraints for pure in-plane bending motion. Appl. Sci. 9 (15), 2999.

Surmeneva, M.A., Koptyug, A., Khrapov, D., Ivanov, Y.F., Mishurova, T., Evsevleev, S., Prymak, O., Loza, K., Epple, M., Bruno, G., et al., 2020. In situ synthesis of a binary Ti–10at% Nb alloy by electron beam melting using a mixture of elemental niobium and titanium powders. J. Mater Process. Technol. 282, 116646.

Tang, D., Yang, C., Geva, T., Del Nido, P.J., 2007. Two-layer passive/active anisotropic fsi models with fiber orientation: mri-based patient-specific modeling of right ventricular response to pulmonary valve insertion surgery. Mol. Cell. Biomech. 4 (3), 159.

Tohgo, K., Wang, A.S., Chou, T.-W., 1993. A criterion for splitting crack initiation in unidirectional fiber-reinforced composites. J. Compos. Mater. 27 (11), 1054–1076.

Tse, Z., Chen, Y., Hovet, S., Monfaredi, R., Xu, S., Wood, B., Cleary, K., 2018. Soft robotics in medical applications. J. Med. Robot. Res. 03, http://dx.doi.org/10.1142/S2424905X18410064.

Vanneste, F., Goury, O., Martinez, J., Lefebvre, S., Delingette, H., Duriez, C., 2020. Anisotropic soft robots based on 3D printed meso-structured materials: design, modeling by homogenization and simulation. IEEE Robot. Autom. Lett. 5 (2), 2380–2386.

Victor, A., Ribeiro, J., Araújo, F.F., 2019. Study of pdms characterization and its applications in biomedicine: A review. J. Mech. Eng. Biomech. 4 (1), 1–9.

Vignali, E., Gasparotti, E., Capellini, K., Fanni, B.M., Landini, L., Positano, V., Celi, S., 2020. Modeling biomechanical interaction between soft tissue and soft robotic instruments: importance of constitutive anisotropic hyperelastic formulations. Int. J. Robot. Res. 0278364920927476.

Wu, W., Geng, P., Li, G., Zhao, D., Zhang, H., Zhao, J., 2015. Influence of layer thickness and raster angle on the mechanical properties of 3D-printed peek and a comparative mechanical study between peek and abs. Materials 8 (9), 5834–5846.

Wu, W., Ye, W., Wu, Z., Geng, P., Wang, Y., Zhao, J., 2017. Influence of layer thickness, raster angle, deformation temperature and recovery temperature on the shape-memory effect of 3D-printed polylactic acid samples. Materials 10 (8), 970.

Zhao, Y., Chen, Y., Zhou, Y., 2019. Novel mechanical models of tensile strength and elastic property of fdm am pla materials: Experimental and theoretical analyses. Mater. Des. 181, 108089.

Zhou, J., Khodakov, D.A., Ellis, A.V., Voelcker, N.H., 2012. Surface modification for pdms-based microfluidic devices. Electrophoresis 33 (1), 89–104.